Depletion of tumor-reactive HSCs reveals their significance during different stages of liver metastasis

VISUAL ABSTRACT

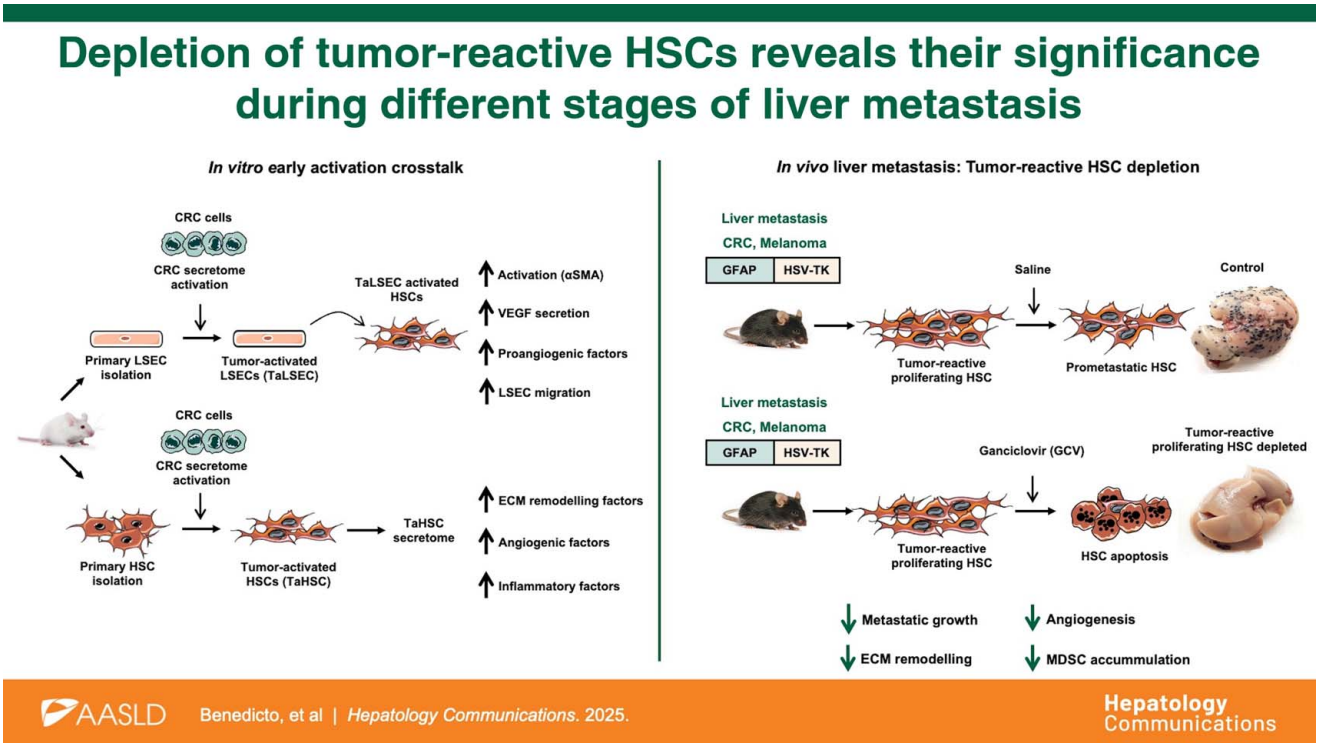

Received: 17 July 2024 | Accepted: 16 December 2024

DOI: 10.1097/HC9.0000000000000669

ORIGINAL ARTICLE

OPEN

Depletion of tumor-reactive HSCs reveals their significance during different stages of liver metastasis

Aitor Benedicto[1] | **Alba Herrero**[2] | **Aritz Lopategi**[3] | **Scott L. Friedman**[4] | **Maria Dolores Boyano**[2] | **Beatriz Arteta**[2]

[1]Cell Biology and `Histology Department, School of Pharmacy, University of the Basque Country, UPV/EHU, Vitoria-Gazteiz, Spain

[2]Cell Biology and Histology Department, School of Medicine and Nursing, University of the Basque Country, UPV/EHU, Leioa, Spain

[3]Physiology Department, School of Medicine and Nursing, University of the Basque Country, UPV/EHU, Leioa, Spain

[4]Division of Liver Diseases, Icahn School of Medicine at Mount Sinai, New York City, New York, USA

Correspondence
Beatriz Arteta Ruiz, Cell Biology and Histology Department, School of Medicine and Nursing, University of the Basque Country, UPV/EHU, Leioa 48960, Vitoria-Gazteiz, Spain.
Email: beatriz.arteta@ehu.eus

Abstract

Background: Activated HSCs play a major role in tissue repair, extracellular matrix regulation, immune response, and inflammation. However, their contributions to the hepatic tumor microenvironment are underexplored and need to be clarified.

Methods: In vitro, we analyzed the responses of freshly isolated LSECs and HSCs to tumor cell supernatants and secretome-driven activation of both primary cell types. For in vivo HSC depletion, transgenic mice expressing the herpes simplex virus-thymidine kinase (HSV-Tk) gene driven by the mouse glial fibrillary acidic protein promoter were used. MC38 colon carcinoma or B16 melanoma was intrasplenically injected to generate liver metastasis to further analyze metastatic growth, collagen accumulation, angiogenesis, and immunosuppression.

Results: Metastatic tumor cells arrest and adhere in the liver 48 hours after intrasplenic injection. The 65% of arrested tumor cells were surrounded by α-smooth muscle actin–expressing cells. In vitro, tumor-activated LSEC-derived secretomes stimulated α-smooth muscle actin expression, migration, VEGF, and LSEC promigratory factor release by HSCs. Tumor cell secretomes stimulated HSC proliferation and the secretion of proangiogenic and protumoral mediators. HSC depletion reduced the foci number and metastatic area in colorectal cancer and melanoma models. Moreover, livers from transgenic mice showed reduced key tumor microenvironment parameters, including intratumoral collagen accumulation, neoangiogenesis, and recruitment of myeloid-derived suppressor cells.

Conclusions: Depletion of tumor-reactive proliferating HSCs implicates these cells as the required spark for the initiation and progression of liver metastasis,

Abbreviations: αSMA, α-smooth muscle actin; aHSC, activated HSC; cHSCs, control HSCs; CRC, colorectal cancer; ECM, extracellular matrix; GCV, ganciclovir; GFAP, glial fibrillary acidic protein; HSV-Tk, herpes simplex virus thymidine kinase gene; MDSC, myeloid-derived suppressor cells; MMP, metalloprotease; TaHSCs, tumor-activated HSCs; TaLSECs, tumor-activated LSECs; TG, transgenic; WT, wild type.

Supplemental Digital Content is available for this article. Direct URL citations are provided in the HTML and PDF versions of this article on the journal's website, www.hepcommjournal.com.

making them a good candidate for new therapies targeting the tumor microenvironment to treat liver metastasis of different primary origins.

Keywords: angiogenesis, CRC, LSEC, melanoma, tumor microenvironment

INTRODUCTION

HSCs are non-parenchymal liver resident cells with a wide array of functions.[1] HSCs populate the space of Disse, in close contact with hepatocytes and LSECs. However, pathogenic stimuli promote HSC activation (aHSC), characterized by transdifferentiation from a quiescence state toward a myofibroblast-like cell. Once activated, aHSCs play a major role in tissue repair, extracellular matrix (ECM) regulation, immune response, and inflammation. The role of aHSCs in liver fibrosis has been extensively characterized.[2] More recent data implicate HSC in the development of primary and metastatic liver cancer.[3–7] Recent studies show that HSCs promote liver metastasis through the CCL20/CCR6 axis and retinoic acid secretion in colorectal cancer (CRC) and pancreatic cancer, respectively.[8,9] Moreover, a recent study related to HGF secretion by aHSCs promotes gastric cancer invasion and liver metastasis.[10] Despite this, the contribution of HSCs to modulating the liver microenvironment during metastasis development is inadequately explored.

The crosstalk during the early stages of liver metastasis engages the activation of LSECs,[11,12] which in turn may mediate the activation of HSCs to support tumor growth. We aim to decipher the participation of HSCs during early liver metastasis in vitro by incubating freshly isolated primary mouse LSECs and HSCs with cancer cells and also model late metastatic growth using an in vivo approach by selectively depleting proliferating HSCs. Elimination of aHSCs has proven successful in uncovering the role of HSCs in liver fibrosis.[2] However, to date no studies have selectively eliminated the aHSCs during metastatic colonization of the liver. Puche et al used a transgenic (TG) model based on the ectopic expression of the herpes simplex virus-thymidine kinase (HSV-Tk) gene using glial fibrillary acidic protein (GFAP) as a promoter. Therefore, HSCs will express HSV-Tk and will, therefore, metabolize ganciclovir (GCV). However, only proliferating GFAP-expressing cells are susceptible to apoptotic cell death upon GCV metabolism due to metabolite toxicity. In rodent liver GFAP is mainly expressed in HSCs;[13] thus, this model is suitable for the study of HSCs in the injured liver. Additionally, this model allows us to eliminate tumor-activated HSCs (TaHSCs) that are in a proliferative state.

METHODS

Animals

Eight to ten-week-old male GFAP-Tk mice (B6.Cg-Tg (Gfap-Tk)7.1Mvs/J, Jackson Laboratory) were used for in vivo experiments. Wild-type (WT) littermates were used as controls. For early tumor cell retention, 6–8-week Balb/c mice were obtained from Charles Rives, syngeneic with CRC CT26 cells. Animal housing, care, and experimental conditions were conducted in conformity with institutional guidelines that are in compliance with the relevant national and international laws and policies.

Cancer cell lines

CT26 CRC murine cell line (ATCC), murine CRC cell line MCA38 (Kerafast) were maintained in RPMI-1640, and melanoma cell line B16-F10 (ATCC, LGC Standards SLU) was maintained in DMEM. The three cell lines were supplemented with 10% fetal bovine serum (FBS), penicillin (100 U/mL), streptomycin (100 μg/mL), and amphotericin B (0.25 μg/mL) (Thermo Fisher Scientific).

Carboxyfluorescein succinimidyl ester vital probe labeled cancer cell retention in the sinusoid and αSMA immunohistochemistry

Detailed description in additional methodological details, http://links.lww.com/HC9/B948.

Tumor-derived secretomes

A total of 1×10^5 cells were cultured in 24 well plates overnight in a complete growth medium. Afterward, cells were cultured in a serum-free medium for 24 hours, and the supernatants or conditioned medium were collected and centrifuged at 4000 rpm for 5 minutes to eliminate any cell debris. The supernatants were kept at −20 °C.

Isolation and primary culture of hepatic sinusoidal cells

Mouse liver perfusion, isolation, and primary culture of liver sinusoidal cells have been described elsewhere[9]

(additional methodological details, http://links.lww.com/HC9/B948).

HSC secretome analysis

Detailed description in additional methodological details, http://links.lww.com/HC9/B948.

Flow cytometric analyses

HSC cells were first incubated for 30 minutes at 4 °C with 1 μg/10^6 cells of mouse anti–α-smooth muscle actin (αSMA) antibody (Dako) followed by conjugated Alexa 488-IgG2a anti-mouse antibody labeling (Invitrogen). Cells were then analyzed by flow cytometry using a FACS Vantage SE flow cytometer (Becton Dickinson) by using a wavelength analysis (green: 530 nm) after excitation with 488 nm light. Dead cells ($<10\%$) were excluded from the analysis using Viaprobe (Becton Dickinson).

In vitro migration assay

LSEC and HSC cell migration assays were performed using modified Boyden chambers as previously described.[5,9] Detailed description in additional methodological details, http://links.lww.com/HC9/B948.

Measurement of VEGF and IL-6 concentration

Detailed description in additional methodological details, http://links.lww.com/HC9/B948.

Quantification of HSC proliferation upon tumor-derived secretome activation

Freshly isolated HSCs were cultured in 48 plate wells for 18 hours in serum-free conditions. Then, HSCs were cultured for 4 days in the presence of RPMI 1% FBS, MCA38-derived and B16-derived secretomes, and diluted 1:2 in 1% FBS and gentamycin-supplemented medium. Afterward, cell viability was assessed using PrestoBlue Viability Reagent (Thermo Fisher Scientific). Briefly, PrestoBlue was diluted 1:10 in fresh medium and incubated for 3 hours with HSCs. Then, the absorbance was measured through Gen5 Software (Agilent BioTek). The absorbance was linked with cell number through a standard curve to calculate HSC number and proliferation. All treatment routines were compared to untreated control cells (both WT-HSCs and TG-HSCs) and considered 100% viability.

Selective in vitro killing of HSCs-TK cells by GCV

Freshly isolated HSCs from WT and *HSCs-TK* (TG) littermates were cultured for 18 hours in 48 well plates under serum-free conditions. Afterward, the medium was replaced with fresh RPMI medium supplemented with 1% FBS and gentamycin. HSCs were cultured in the presence of either the control medium or MCA38 or B16-F10 derived secretomes (diluted 1:2 in 1% FBS containing RPMI medium). Cultures were then supplemented with either 5 μM GCV solution or saline solution (0.9% NaCl) for 4 days. Finally, cell viability was quantified using PrestoBlue viability assay as previously specified. Cell viability was calculated using WT-HSCs and TG-HSCs under control conditions as a reference.

Liver metastasis assay

Murine MCA38 CRC cells or B16-F10 melanoma cells were diluted in PBS (2×10^6 cells/mL), and 100 μL of the cell solution was intrasplenically injected. Littermates were divided into 4 groups ($n=4$) based on their genotype and GCV treatment schedule (Supplemental Figure S1, http://links.lww.com/HC9/B934). Paraffin-embedded liver sections, 10 μm thick, were stained using hematoxylin and eosin for the metastatic area and foci number quantification. Three different liver sections were analyzed separated by 500 μm between each other. In vivo assays were carried out 2 times ($n=8$/group).

In vivo HSC selective killing

Mice received i.p. injections of GCV (100 μg/g/day) (200 μL) or saline from day 5 to day 13. This GCV concentration effectively eliminates proliferating HSCs without toxic effects.[2]

Western blot analysis

Western Blot procedure has been detailed elsewhere.[5]

In vitro detection of cell apoptosis by immunofluorescence

Detailed description in additional methodological details, http://links.lww.com/HC9/B948.

Immunohistochemistry

For collagen accumulation, picrosirius red staining was utilized in liver paraffin sections.[5] Two sections

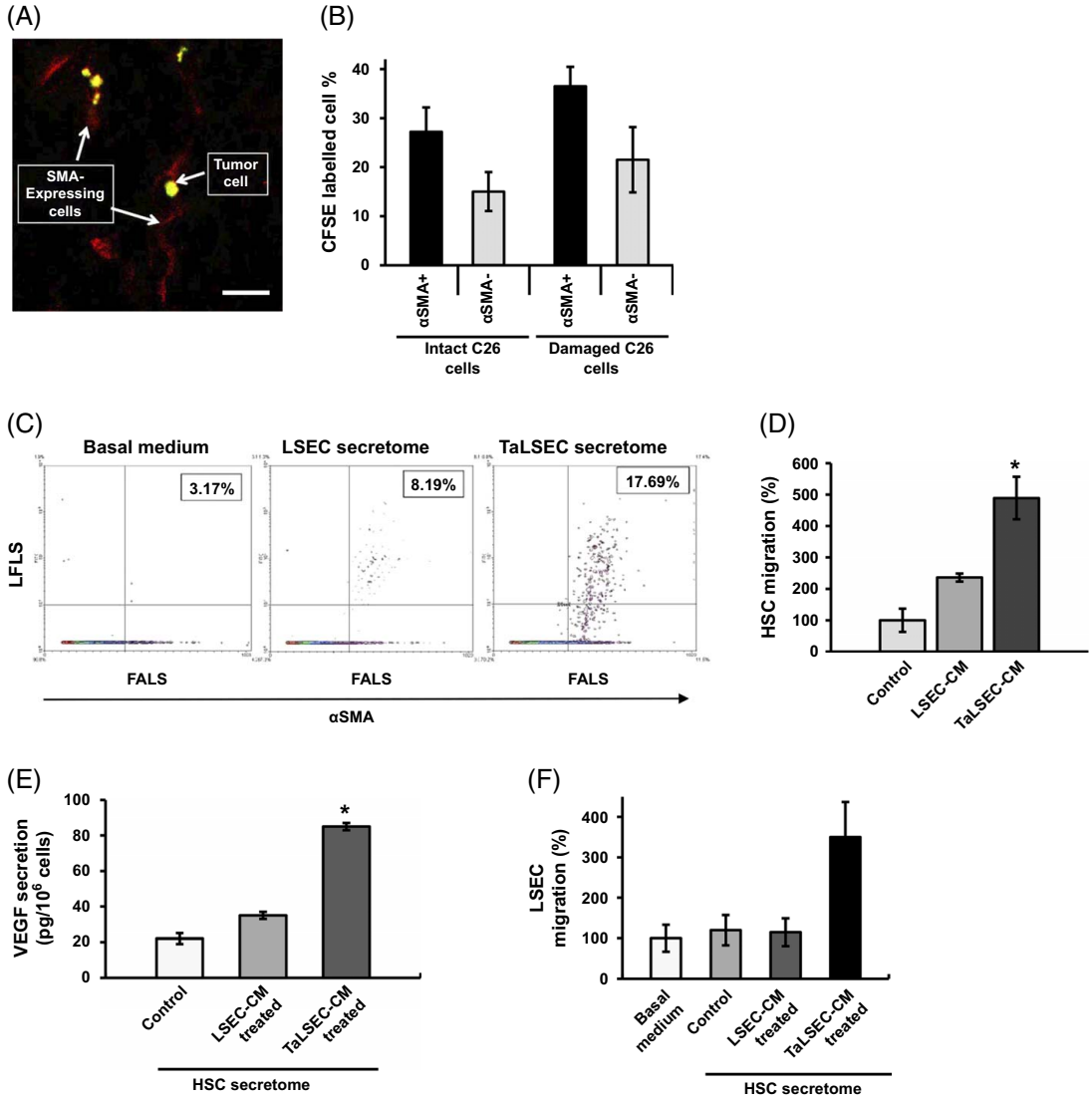

FIGURE 1 Cancer cell adhesion during liver colonization and crosstalk to initiate metastasis. αSMA (red)-expressing cells localize in contact with CFSE (green)-labeled CT26 cells (A, B). HSC activation mediated by TaLSECs quantified by αSMA expression (C). Migration of HSCs treated with control medium and LSEC-derived secretome and TaLSEC-derived secretome (D). VEGF secretion by HSCs under control, LSEC secretome stimulation, and TaLSEC secretome stimulation (E). LSEC migration treated with control, LSEC secretome–activated HSCs supernatants, and TaLSEC secretome–activated HSCs supernatants (F). Data were considered statistically significant for $*p < 0.05$ using a one-tailed Mann–Whitney test. Scale bar: 50 μm. Abbreviations: αSMA, α-smooth muscle actin; CFSE, carboxyfluorescein succinimidyl ester; FALS, forward angle light scatter; LFLS, Diffraction light intensity log; LSEC-CM, LSEC conditioned-media; TaLSECs, tumor-activated LSECs.

separated by 500 μm were analyzed from each liver (n = 6/group).

Frozen tissue Immunohistochemistry

The protocol is detailed elsewhere.[4] αSMA incubated samples were washed, blocked, and incubated with anti-mouse CD31 (1:500) for 2 hours followed by Alexa fluor 488 incubation. Sections were mounted using a DAPI-containing fluoromount (Abcam) and visualized under an Axioscope Fluorescent microscope. Two sections separated by 500 μm were analyzed from each liver (n = 6/group).

Gene expression quantification

Detailed description in additional methodological details, http://links.lww.com/HC9/B948.

Statistical analyses

Data were expressed as means ± SD. Statistical analysis was performed by SPPS statistical software for MS Windows, release 13.0 (Professional Statistic). For different group comparisons and 2 categoric variables, two-way ANOVA was carried out. For single comparisons (treatment vs. control), a one-tailed Mann–Whitney no

parametric test was carried out. The criterion for significance was at least $p \leq 0.05$ for all comparisons. Unless stated, all the experiments were performed in triplicate.

RESULTS

αSMA-expressing cells co-localized with intrasinusoidally arrested CT26 cancer cells within the hepatic microvasculature

Tumor cell retention in the liver occurs in the sinusoids. Here we observed that 48 hours after the injection, αSMA-expressing cells mainly co-localized with intrasinusoidally arrested both intact and damaged CT26 cells (Figures 1A and B) and rarely occurred around tumor-unaffected sinusoidal segments. However, up to 35% of the arrested cancer cells were not associated with αSMA-positive cells (Figure 1B), indicating either later recruitment or absence of αSMA-expressing cells during this very early stage of liver invasion.

LSECs act as activators and recruiters of αSMA-expressing HSCs in the early stage of liver metastasis

LSECs represent the first barrier for the circulating tumor cell when invading the liver, and tumor-endothelial crosstalk facilitates the metastatic process.[1] Therefore, it is tempting to hypothesize that tumor activation of LSECs may precede the recruitment of HSCs to the nascent foci. Indeed, in vitro activation of isolated primary mouse HSC with secretomes from in vitro tumor-activated freshly isolated LSECs (TaLSEC) promoted αSMA expression in primary HSCs in vitro 5-fold compared to non-stimulated HSCs (Figure 1C). To further analyze the involvement of TaLSECs in the recruitment of HSCs into the early metastatic niche, we analyzed the migration of HSCs under basal conditions, LSEC-secretomes activation, and TaLSEC-secretomes activation. LSEC secretomes boosted HSC migration by 2-fold compared to the basal medium (Figure 1D). Furthermore, we reported a 2-fold increased migration of HSCs when stimulated with TaLSEC secretomes, compared to that of control LSECs (Figure 1D). Interestingly, this TaLSEC-mediated aHSC promoted the secretion of VEGF by aHSCs. In detail, VEGF was increased 4-fold in TaLSEC secretome-treated HSCs in vitro (Figure 1E), confirming TaLSEC-driven activation of HSC during early stages of liver metastasis. Finally, we observed that the soluble factors released by HSC activated with TaLSEC secretomes promote the migration of LSECs 3.5-fold compared to control HSCs (cHSCs) (Figure 1E), confirming the angiogenic crosstalk between invading cancer cells, LSECs, and HSCs during early colonization of the liver.

Tumor cell interplay with HSC boosts their GFAP expression and proliferation

In the liver, GFAP is constitutively expressed in most HSCs and is increased upon activation.[3] Here we show that soluble factors released from CRC MCA38 cancer cells mediate the upregulation of GFAP protein in vitro. As observed in Figure 2A, immunofluorescence analysis revealed higher GFAP expression in vitro TaHSCs than in control primary HSCs (cHSCs). In line with this result, western blot analysis revealed a 3-fold increase in GFAP protein level in TaHSCs upon stimulation with tumor-derived secretomes compared to control ones (Figure 2B). Further in vivo inmunohistochemical analysis shows high GFAP expression in peritumoral HSC during liver metastasis of B16 melanoma and CRC (Figure 2C), along with GFAP expression in infiltrating HSCs (Figure 2C, white arrows). In line with this result, GFAP RNA expression was increased by 3-fold in TaHSCs compared to cHSCs in vitro (Figure 2D). Along with the upregulation of this cytoskeletal marker, tumor-derived secretomes stimulated the proliferation of primary mouse HSC in both CRC and melanoma models (Figure 2E). In detail, the freshly isolated primary mouse HSC cell number increased by 50% after 4 days of incubation with tumor-derived secretomes compared to control primary HSCs. Proliferation is essential for the activity of the TG model since TaHSCs increase GFAP expression and proliferate, both requirements for the proper function of the GFAP-Tk model for the depletion of TaHSCs during liver metastasis.

Tumor secretomes–mediated proliferation renders HSCs susceptible to selective killing by GCV

As previously shown, cultured TaHSCs proliferate more than untreated HSCs. To further validate the model for liver metastasis, we analyzed the effect of GCV in freshly isolated HSCs treated with tumor secretomes. Here, we show that GCV treatment neither affected the viability of HSCs isolated from WT littermate mice nor of untreated HSCs nor that of TaHSCs (Figure 3A) after 4 days in culture. However, GCV was cytotoxic to HSCs isolated from TG mice. More specifically, GCV slightly affected TG cHSCs, being much more effective in MCA38 and B16-F10 secretomes–treated TG primary HSCs (Figure 3B, squares 6 and 9). Cell viability analysis revealed a significant 70% reduction in viable TaHSCs compared to control TG HSC challenged with GCV. This finding confirms the selective killing of proliferating TaHSC upon GCV treatment. Saline control did not affect HSC viability in any treatment routine. To deepen the mechanisms behind this selective cell death, immunohistochemical analyses were conducted in both WT and TG mice isolated HSC stimulated with tumor-derived secretomes for 4 days. As represented in Figure 3C, the expression of

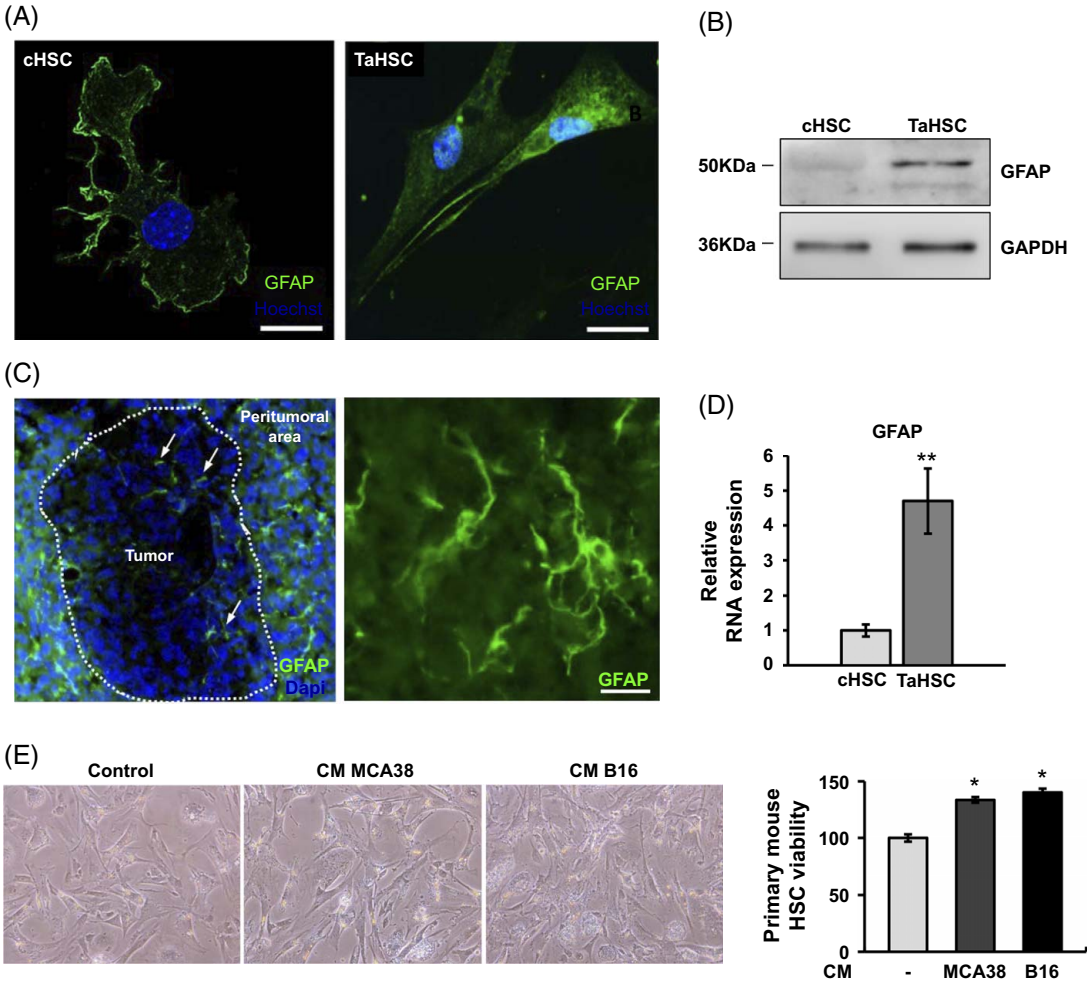

FIGURE 2 Tumor-mediated GFAP expression and proliferation in HSCs. The expression of GFAP (green) was analyzed in cHSC and TaHSCs through immunofluorescence (A) and western blot (B). Nuclei were stained with DAPI-containing mounting media. Scale bar: 10 μm. Peritumoral and Intratumoral (white arrows) GFAP expression (green) was analyzed in vivo by immunohistochemistry. Nuclei were stained with DAPI-containing mounting media (C). Scale bar: 10 μm. GFAP expression in primary HSCs treated with a control medium or tumor-derived secretomes was analyzed (D). Data were considered statistically significant for $^{**}p < 0.01$ using the one-tailed Mann–Whitney test. HSC proliferation was measured after 4 days of culture with tumor-derived secretomes. A total of 4×10^4 freshly isolated HSCs were cultured for 18 hours, after which the media was changed for the appropriate treatment. After 4 days, cell viability was measured. Obtained absorbance was linked with cell number using a standard curve (E). Data were considered statistically significant for $^{*}p < 0.05$ using the one-tailed Mann–Whitney test. Abbreviations: cHSC, control HSC; GAPDH, glyceraldehyde-3-phosphate dehydrogenase; GFAP, glial fibrillary acidic protein; TaHSC, tumor-activated HSC.

proapoptotic protein caspase-3 was absent in WT TaHSC cultures, while cell morphology and nuclei appearance were not affected. However, TG-isolated TaHSC presented high levels of apoptotic cell death. On the one hand, caspase-3 expression was present in a high percentage of cells, while on the other hand, nuclei condensation and myofibroblast-like shape loss were notable, with pronounced shrinkage of cell cytoplasm and nuclei condensation (Figure 3C).

Selective killing of TaHSCs reduces liver metastasis

As shown before, αSMA-expressing sinusoidal cells (HSCs) are in close contact with tumor cells 48 hours after tumor cell injection. The interplay with both tumor cells and, especially, LSECs, initiates angiogenic reaction in the nascent foci, a key requirement for tumor growth.[14] To further clarify the involvement of HSCs in the development of liver metastasis, an in vivo assay was performed using the GFAP-Tk mice model. Following specific depletion of tumor-reactive proliferating HSCs (checked by αSMA quantification in the metastatic foci, Supplemental Figure S2, http://links.lww.com/HC9/B934), there was a significant and relevant role of these pericyte-like cells during the metastatic growth of both MCA38 CRC and B16-F10 melanoma cells in the liver. WT mice treated either with saline or GCV showed high liver colonization after 14 days, while TG mice treated with saline exhibited the same invasion pattern. On the contrary, GCV

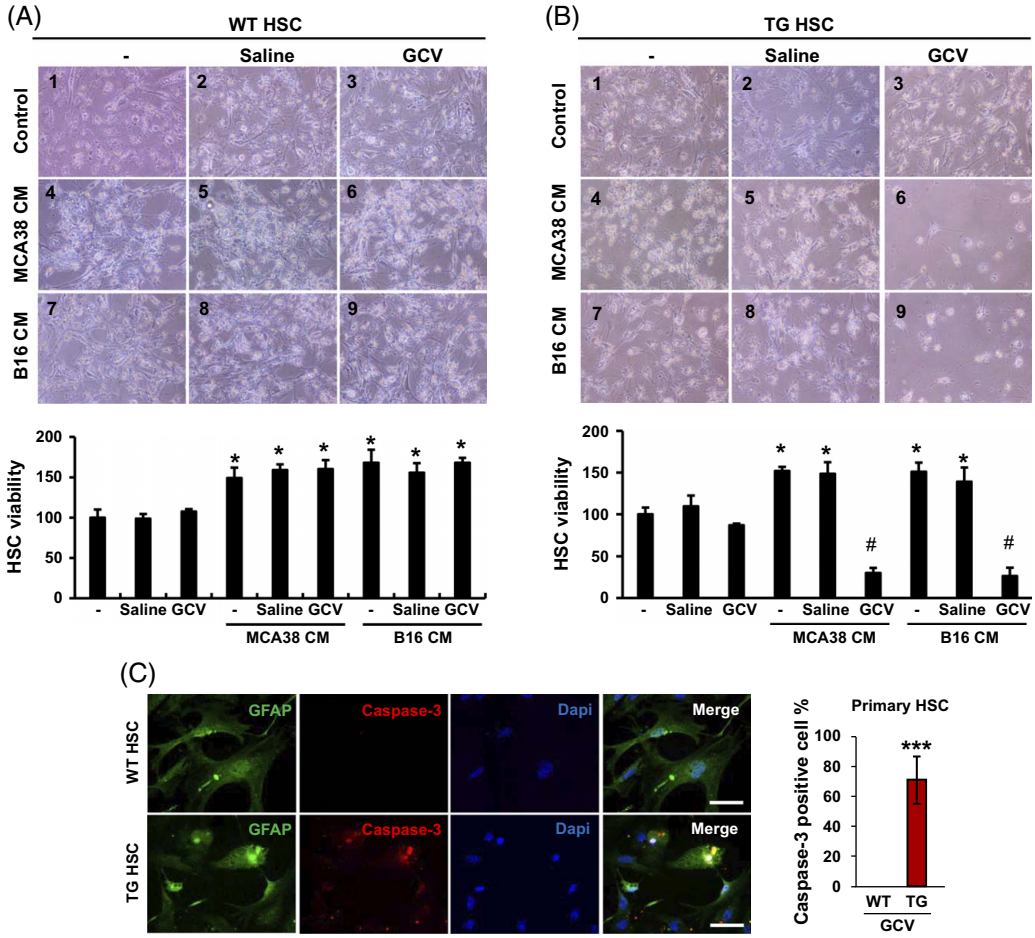

FIGURE 3 GCV promotes TaHSC cell death in TG mice. Both WT (A) and TG (B) mice isolated HSCs were treated with MCA38 (MCA38 CM) and B16-F10-derived secretomes (B16 CM) for 4 days. HSCs were also challenged with saline and GCV (5 μM) to analyze cell death. Differences between control-derived and tumor-derived secretome-treated HSCs were considered statistically significant for $*p < 0.05$ using the Student *t* test. Differences between saline and GCV-treated HSCs were considered statistically significant for $\#p < 0.01$ using the Student *t* test. 1—control HSC, 2—control cells + saline, 3—control HSC + GCV, 4—MCA38 CM–treated HSC, 5—MCA38 CM + saline-treated HSC, 6—MCA38 CM + GCV-treated HSC, 7—B16 CM–treated HSC, 8—B16 CM + saline-treated HSC, 9—B16 CM + GCV-treated HSC. Cell death was analyzed in TaHSC after 5 days in culture through caspase-3 detection (red). Treatment versus control data were considered statistically significant for $p < 0.05$ using a two-way ANOVA test. GCV-treated versus saline-treated in TG HSCs was considered statistically significant for $\#p < 0.01$ using one-tailed Mann–Whitney test (C). The cells were labeled for GFAP (green) for HSC detection and DAPI (blue) for nuclei visualization. Data were considered statistically significant for the $p < 0.001$ one-tailed Mann–Whitney test. Scale bar: 50 μm. Abbreviations: GCV, ganciclovir; GFAP, glial fibrillary acidic protein; TaHSC, tumor-activated HSC; TG, transgenic; WT, wild type.

treatment almost completely reduced the metastatic development in both tumor models. The metastatic area in the liver was reduced by 85% and 90% in MCA38 CRC and B16-F10 melanoma models, respectively (Figures 4A and C). Selective depletion of TaHSC during liver colonization not only reduced metastatic area but also the number of metastatic foci. CRC metastatic area was decreased by 3-fold in TG treated with GCV compared to the other treatment routines (Figure 4B), while melanoma metastatic foci were reduced 4-fold in the liver of TG mice under GCV treatment (Figure 4D and Supplemental Figure S3, http://links.lww.com/HC9/B934). Differences in the metastatic area were not produced by GCV toxicity against tumor cells, as high doses of GCV did not reduce tumor cell viability in vitro (Supplemental Figure S4, http://links.lww.com/HC9/B934).

Tumor-reactive HSC depletion alters ECM remodeling in the metastatic niche

In the liver, HSCs represent the main ECM source, since they secrete collagen during the development of liver cancer and metastasis.[6] We further explored the involvement of HSCs during liver metastasis by means of intratumoral collagen accumulation and secretion of matrix remodeling soluble factors. Picrosirius red staining revealed a characteristic collagen accumulation around the inner limit of the foci especially in CRC,

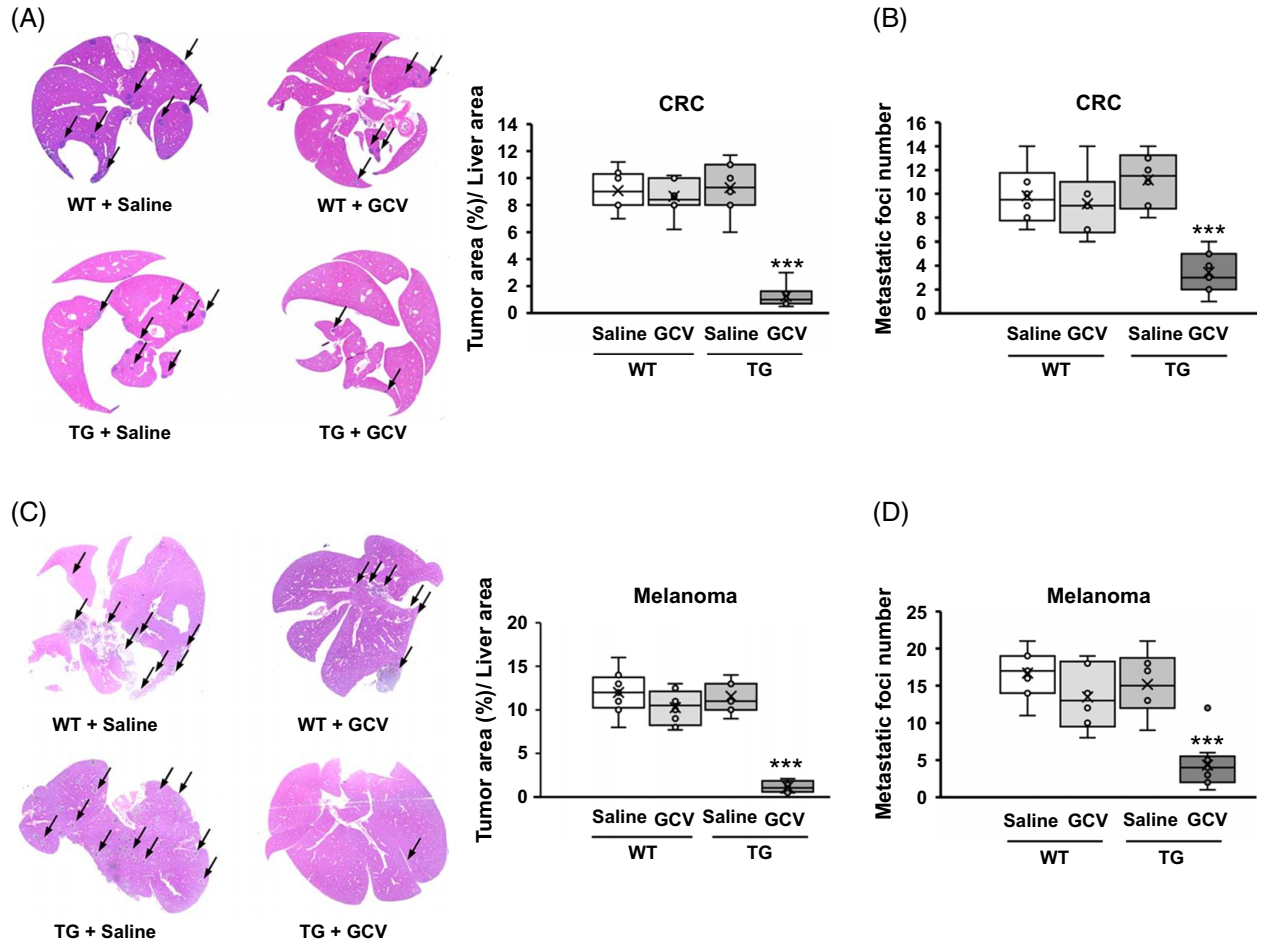

FIGURE 4 Selective depletion of reactive HSCs impairs liver metastasis. The development of liver metastasis of CRC (A) and melanoma (C) was dramatically reduced in mice lacking reactive HSCs upon GCV administration. The other groups showed similar tumor growth independent of the treatment routine and genotype. Differences between control groups and reactive HSCs-depleted mice (TG mice subjected to GCV treatment) were considered statistically significant for ***$p < 0.001$ using the two-way ANOVA test. Abbreviations: CRC, colorectal cancer; GCV, ganciclovir; TG, transgenic; WT, wild type.

along with intratumoral collagen areas. Our data reveals that selectively depleting proliferating HSCs through GCV treatment effectively reduced fibrillar deposition in TG mice. In fact, GCV treatment promoted a 50% reduction in collagen accumulation in CRC liver metastatic foci, as observed through Sirius red, compared to the groups with no HSC depletion (Figure 5A). To note that fibrillar collagen followed a specific pattern in CRC, with accumulation in the inner limit of the metastatic foci. The same trend was observed in melanoma, with half the intratumoral fibrillar collagen accumulation with a more centered intratumoral pattern (Figure 5B). The reduction was more evident in the CRC model using MCA38 rather than in B16-F10 melanoma. Moreover, the ECM remodeling by HSCs is not limited to collagen production. In fact, by secretome analysis there was increased secretion of remodeling proteins by primary TaHSCs in vitro. Twenty-four-hour activation with secretomes from MCA38 CRC cells increased the secretion of metalloprotease (MMP)-3 and MMP-9 around 80 and 2.8-fold respectively, in freshly isolated primary mouse TaHSCs compared to cHSCs. Besides, the secretion of TIMP-1 was stimulated in TaHSCs by 79% compared to cHSCs (Figure 5C).

TaHSC ablation impairs tumor angiogenesis

We have previously shown a close interplay between LSECs and HSCs, driving reciprocal activation and migration (Figure 1). Here we show that treatment of TG mice with GCV during liver metastasis reduced the infiltration of αSMA-expressing cells in CRC and melanoma liver metastatic foci. This observation correlated with reduced intratumoral expression of CD31, an angiogenic mouse LSEC marker (Figures 6A and B), leading to reduced and shorter colocalization sections in the tumors. Consequently, the length of capillaries formed by these 2 cell populations was reduced in HSC-depleted mouse tumors compared to vehicle-treated tumors (Figures 6A and C). Specifically, CRC tumors with

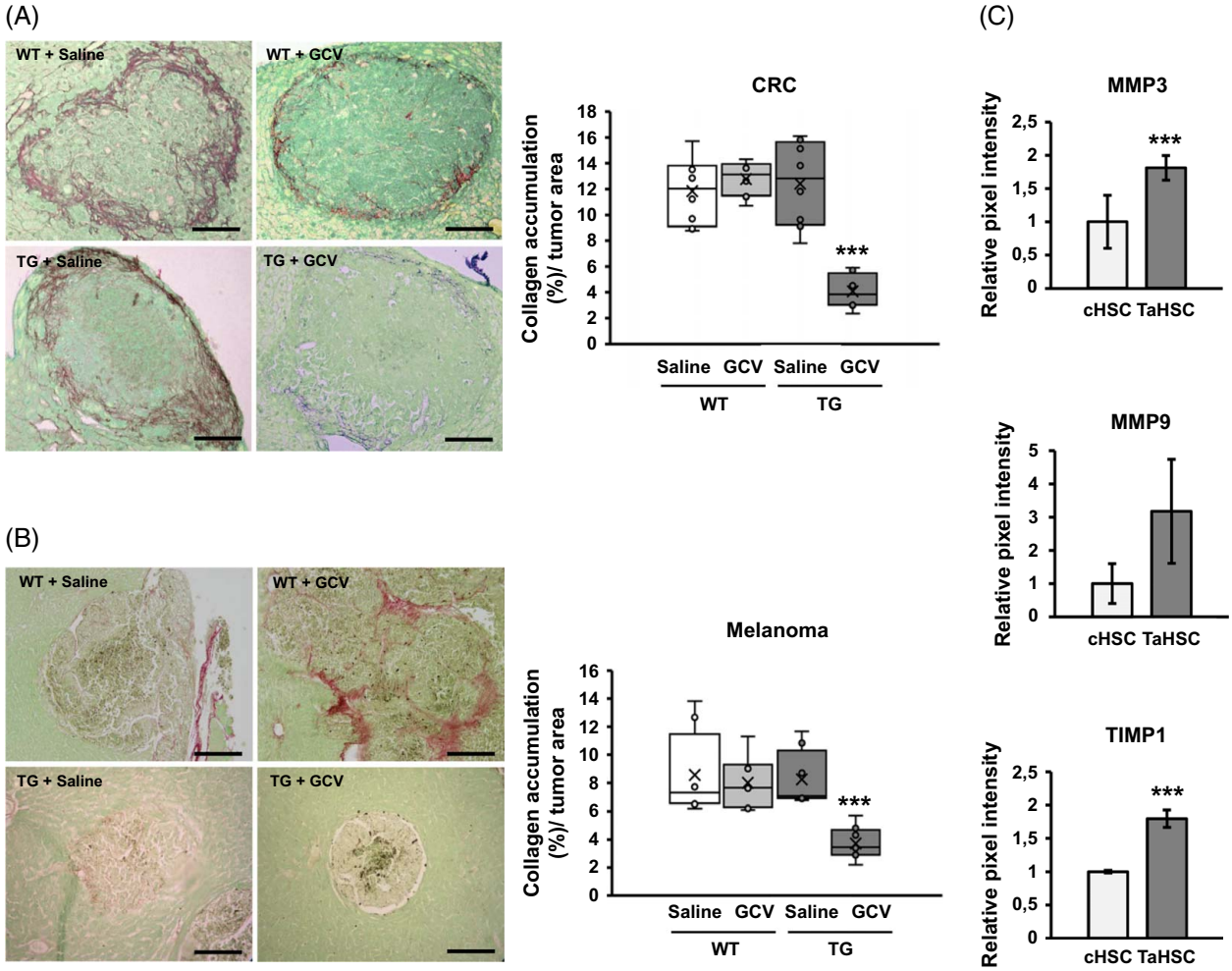

FIGURE 5 ECM reorganization is altered upon HSC depletion. The accumulation of fibrillar collagen was reduced in TG treated with GCV, compared to the other 3 groups (A, B). The secretion of MMPs and TIMP-1 was stimulated by tumor cell secretomes in primary mouse HSCs (C). Differences between control groups and reactive HSCs-depleted mice (TG mice subjected to GCV treatment) were considered statistically significant for ***$p < 0.001$ using a two-way ANOVA test. Differences between cHSC and TaHSC secretion were considered statistically significant for ***$p < 0.001$ using a two-way ANOVA test. Scale bar: 100 μm. Abbreviations: cHSC, control HSCs; CRC, colorectal cancer; ECM, extracellular matrix; GCV, ganciclovir; MMPs, metalloproteases; TaHSC, tumor-activated HSC; TG, transgenic; WT, wild type.

activated and proliferating HSCs displayed an average of 180–210 μm long intratumoral neovessels formed with colocalization of αSMA-expressing and CD31-expressing cells (Figure 6B). However, upon TaHSC elimination, capillaries were dramatically reduced by 75%, with an average of 35 μm long intratumoral capillaries. Regarding melanoma, the same pattern was observed, with 150–160 μm long new vessels in TaHSC-bearing mice compared to 30 μm long vessels in proliferating HSC-depleted mice foci (Figure 6D).

The activation of HSCs with tumor secretomes stimulates the production of proangiogenic factors

In order to identify possible mechanisms driving this angiogenic response dependent on TaHSCs, we further analyzed the secretome of freshly isolated primary mouse HSCs in vitro (Figure 7A) using a *Proteome Profiler Angiogenesis Array Kit*. TaHSCs showed myofibroblastic shape by the time of collection of secretomes (Supplemental Figure S5, http://links.lww.com/HC9/B934). In line with this observation, the results showed increased secretion of several angiogenic factors. Proliferin was stimulated in TaHSCs up to 8-fold. Cyr61 was increased 2-fold and osteopontin was upregulated by 37% in TaHSCs compared to that of cHSCs, showing increased expression in RNA levels too (Supplemental Figure S6, http://links.lww.com/HC9/B934). Thrombospondin increased 24%, HGF 23%, SerpinE1 46%, VEGF 15%, Cyr61 100%, and angiopoietin-1 40% in the supernatants of TaHSCs compared to that of cHSCs (Figure 7E). Therefore, depletion of TaHSC from the tumor microenvironment reduces proangiogenic signals to impair the formation of new intratumoral vessels.

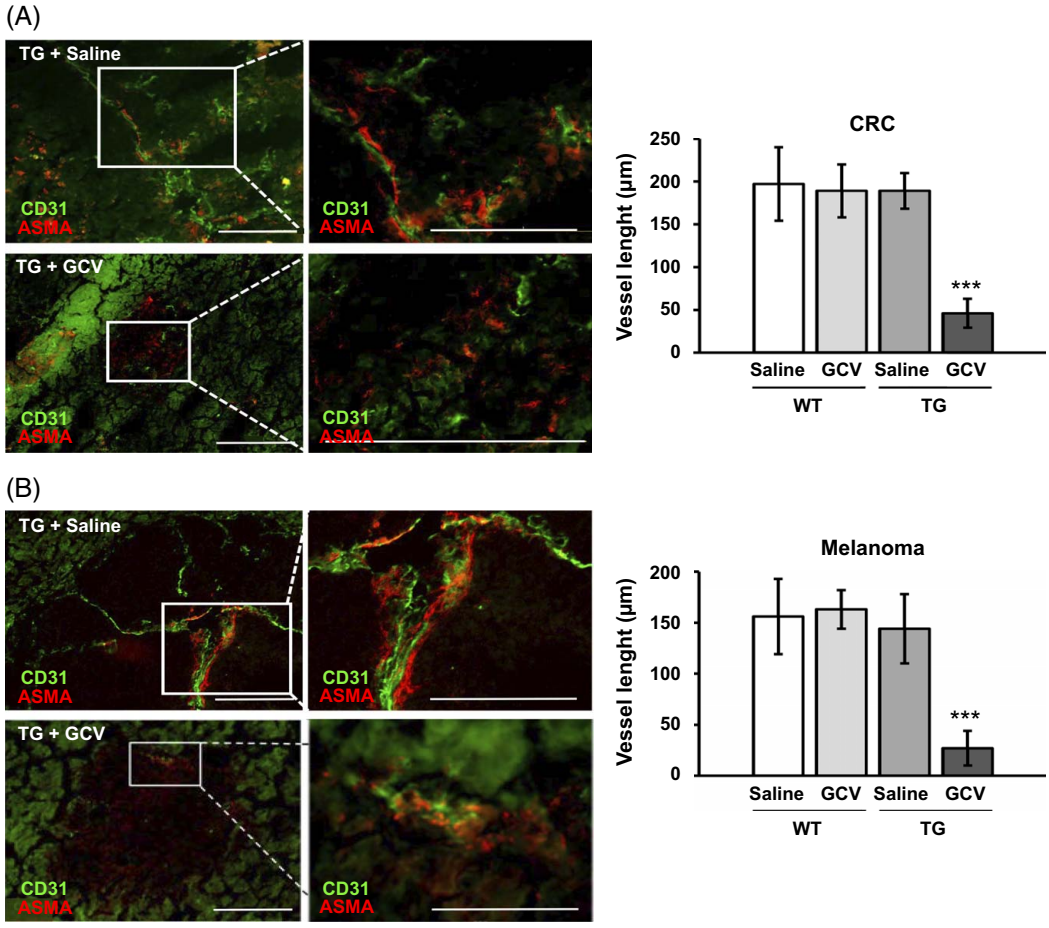

FIGURE 6 Angiogenesis is impaired in HSC-deficient metastatic tumors. Intratumoral expression of angiogenic LSECs, characterized by CD31 (green) and αSMA-expressing activated angiogenic HSC (red) is reduced in TG treated with GCV, compared to the other 3 groups in both CRC (A) and melanoma (B) models. Scale bar: 100 µm. Differences between control groups and reactive HSCs-depleted mice (TG mice subjected to GCV treatment) were considered statistically significant for ***$p < 0.001$ using a two-way ANOVA test. Abbreviations: ASMA, alpha-smooth muscle actin; CRC, colorectal cancer; GCV, ganciclovir; TG, transgenic; WT, wild type.

TaHSC elimination impairs the creation of a supportive immunosuppressed liver microenvironment

HSCs have been linked with the creation of a permissive milieu for tumor cells through the creation of an immune-tolerant hepatic microenvironment.[15,16] This process includes the recruitment of myeloid-derived suppressor cells (MDSC) through CXCL12–CXCR4 axis[17] and other mediators. Here we found that livers subjected to selective depletion of TaHSC exhibited much less permissive liver microenvironment for invading CRC metastatic cells, as the accumulation of MDSC, characterized by the double staining with $CD11b^+$ $Ly6G^+$ (Supplemental Figure S7, http://links.lww.com/HC9/B934) was robustly reduced up to 50% in CRC bearing mice liver (Figure 8A). The same trend was observed in B16 melanoma-bearing mice liver, with a 45% reduction in MDSC counts (Figure 8B). The only group showing significant changes in the MDSC population was the one from TG mice treated with GCV and, therefore, selectively depleted for TaHSCs. Further in vitro analysis revealed increased levels of chemoattractant proteins in TaHSC secretomes (Figure 8C). To sum up, TaHSCs showed 180% augmented IL-6, 320% increased levels of CXCL12, 14% of CCL2, and 18% of CXCL10. Besides, tumor activation of HSC promoted the secretion of CXCL4 up to 20%. All these results suggest a significant role of TaHSCs in the generation of a more permissive liver microenvironment which may potentially promote metastatic growth.

DISCUSSION

Depleting HSC has been a major goal for different groups, leading to a better understanding of their function during liver fibrosis and liver damage.[2,18] HSC have been postulated to play a major role during hepatic malignancies,[19] involved in angiogenesis, ECM dynamics, and immune regulation (120-2219).[20–22]

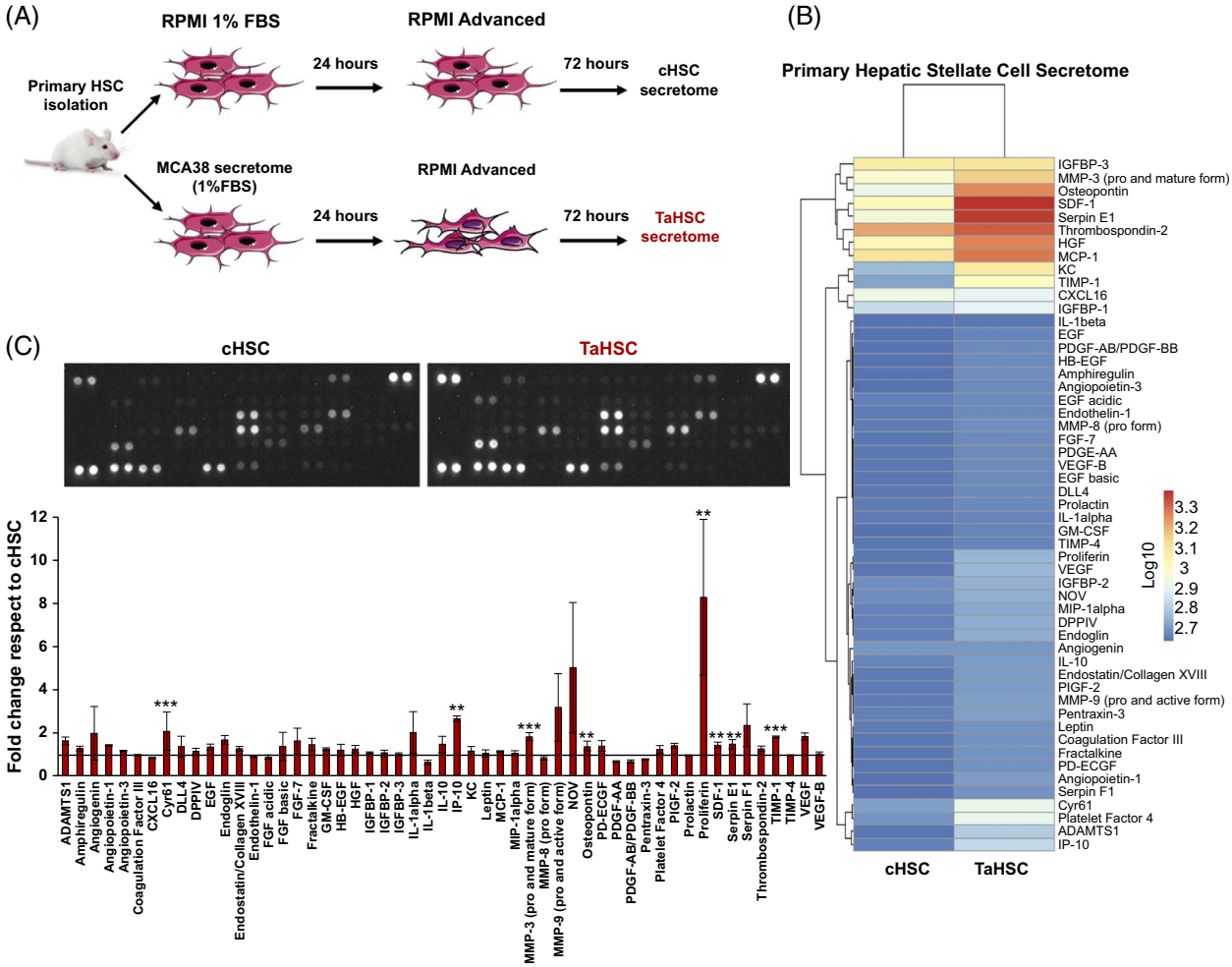

FIGURE 7 Proangiogenic factors released by HSCs are increased after tumor secretome activation. Primary mouse HSCs were cultured for 24 hours and activated for 24 hours with CRC MCA38 cancer cell secretomes. After 72 hours, media was collected (A). Proteome Profiler was carried out, and several angiogenic mediators were upregulated (B, C). Data in the heatmap is represented as the log10 value of the intensities obtained in the Proteome Profiler membranes. Data in the graph is represented as the fold-change for each cytokine compared to the control value. Differences between cHSCs and TaHSCs were considered statistically significant for ***$p < 0.001$ and **$p < 0.01$ using a two-way ANOVA test. Abbreviations: cHSC, control HSC; CRC, colorectal cancer; TaHSC, tumor-activated HSC.

Using intrasplenically injected murine CT26 colon cancer cells, we demonstrated that circulating colon carcinoma cells' interactions with LSECs favor HSC transdifferentiation into myofibroblasts in the early colonization of the liver, within the hepatic microvasculature. Thereafter, αSMA-positive HSCs formed the first premetastatic niche surrounding extravasated cancer cells. In line with these dynamic morphologic data, we showed that the TaLSECs secretomes contained αSMA expression-stimulating factors for quiescent murine HSCs, which suggests that myofibroblastic transdifferentiation accounts for αSMA expression by HSCs located around LSECs cells specifically interacting with circulating CRC cells. TaLSEC cells also released HSC migration-stimulating factors. Moreover, TaLSEC released VEGF secretion-stimulating factors for HSCs, which was consistent with its high endothelial cell migration-stimulating activity, and with previous reports on the proangiogenic role of aHSCs.[23]

We confirmed that tumor cell/HSC crosstalk stimulates GFAP expression in primary mouse HSCs in vitro and in vivo, in line with previous reports.[3] Moreover, CRC and melanoma-derived secretomes increased the proliferation of freshly isolated primary mouse HSC by 50% in vitro, which might be promoted by tumor VEGF.[24] Moreover, viability was reduced by 75% in HSC isolated from TG mice stimulated with tumor-derived secretomes upon GCV treatment. Mechanistically, GCV promoted caspase-3–mediated apoptotic cell death, in line with previous results using this HSC depletion model.[2]

For in vivo assays, we treated mice i.p. for 9 days to observe liver-specific effects and avoid reported unspecific GCV toxicity,[25] (Supplemental Figures S8A and B, http://links.lww.com/HC9/B934).

In vivo depletion of HSCs uncovered HSC-dependent liver metastasis, showing 80% and 90% reduced tumor growth in CRC and melanoma, underscoring a

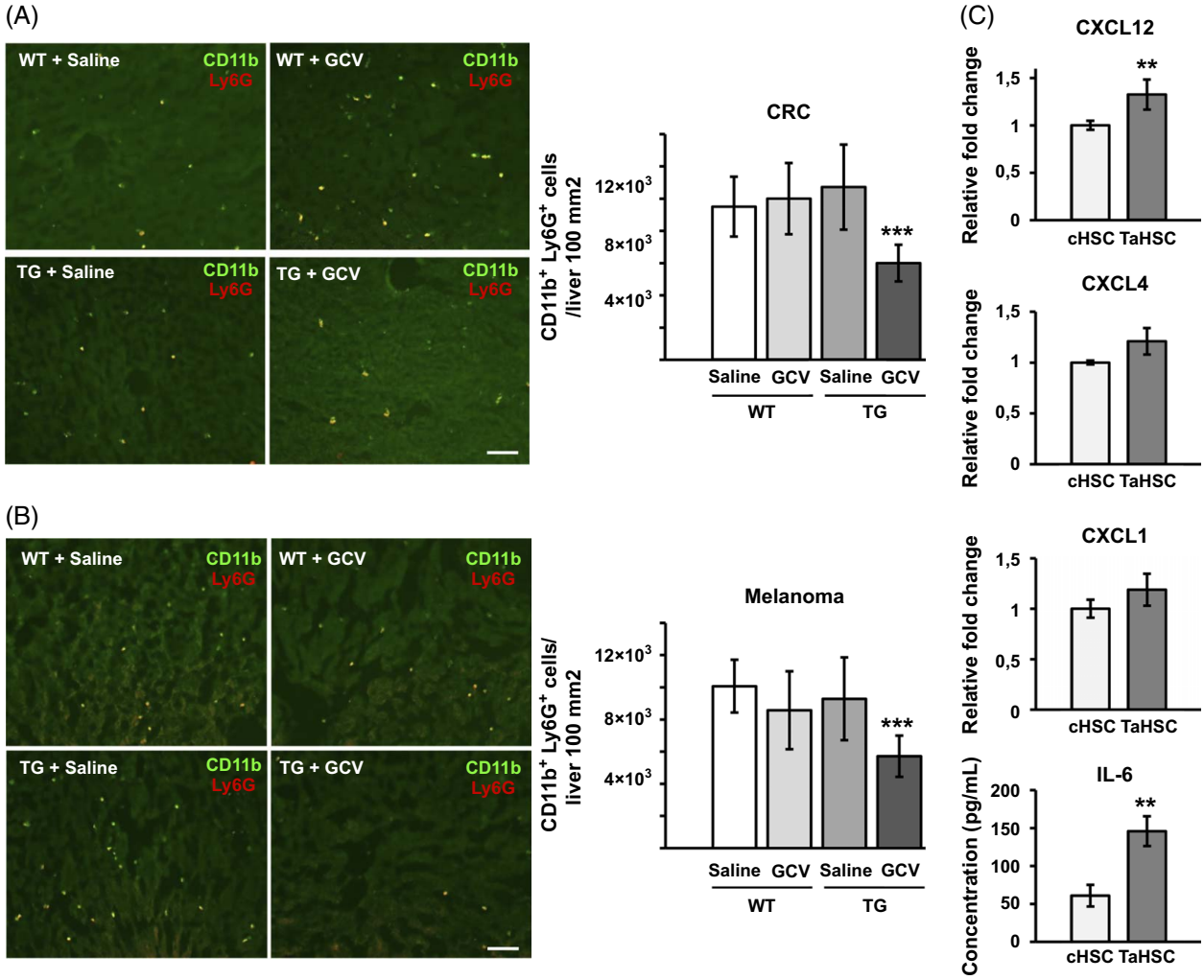

FIGURE 8 MDSC accumulation is impaired in reactive HSC-depleted mice liver. The recruitment of MDSC into the metastatic liver was analyzed in CRC (A) and melanoma (B) tumor models. This process was significantly reduced in mice lacking reactive HSCs upon GCV administration. The other groups exhibited no increased counts of this immunosuppressive population independent of the treatment routine and genotype. Differences between control groups and reactive HSCs-depleted mice (TG mice subjected to GCV treatment) were considered statistically significant for $***p < 0.001$ using a two-way ANOVA test. Scale bar: 100 μm. (C) Relative changes in the secretion of proinflammatory factors by TaHSCs compared to cHSCs. Differences between chemokine and cytokine secretion between cHSCs and TaHSCs were considered statistically significant for $**p < 0.01$ using a two-way ANOVA (CXCL12, CXCL4, and CXCL1) or Mann–Whitney one-tailed test (IL-6). Abbreviations: cHSC, control HSC; CRC, colorectal cancer; GCV, ganciclovir; MDSC, myeloid-derived suppressor cell; TaHSC, tumor-activated HSC; TG, transgenic; WT, wild type.

liver-specific protumoral response, independent from the primary tumor origin. Decreased tumor-reactive HSC number may reduce IL-6, VEGF, and HGF in the tumor microenvironment, upregulated in TaHSCs, impairing metastasis, since these mediators boost tumor growth.[3,26] Even though no study has depleted HSC during liver tumorigenesis, the inhibition of aHSC impaired subcutaneous hepatocarcinoma growth in mice, while HCC/HSC crosstalk favors metastasis of this malignancy, supporting the significant role of HSC in cancer progression.[27,28] Several protumoral processes have been related to HSC, such as tumor cell proliferation, migration, and secretion of proinflammatory cytokines.[6,29] Interestingly, the presence of peritumoral HSC has been related to hepatic recurrence after CRC lesion resection.[30] All these data support the critical role of HSC during liver tumor growth.

Regarding collagen accumulation, the dominant role of HSC during fibrosis and liver scar formation[1] may explain the reduced fibrillar collagen upon HSC depletion. Interestingly, the same reduction in collagen matrix was reported by Puché et al[2] during liver damage, while targeting collagen synthesis in HSC during fibrosis facilitated the resolution of the disease.[31] Moreover, tumor cells stimulate collagen synthesis in HSCs[32] and consequently, the reduction in tumor stimuli may prevent collagen accumulation by not depleting HSCs, since only about 70% of mouse HSC express GFAP and will render to GCV treatment.[2,33]

HSCs are required for neoangiogenesis formation in the metastatic foci,[3,34] where they interact with LSECs to form vessels to supply the growing tumor.[9,33] We reported diminished angiogenesis upon HSC depletion, maybe due to a reduced fibrotic matrix to support new vessels[35] and reduced αSMA-expressing contractile HSCs, which may act as vascular smooth muscle cells that aid in the maintenance and the structure of new vessels as observed in other cancers.[36] Besides, TaHSCs promote the migration of LSECs to form new capillaries through VEGF secretion.[3,12] We demonstrate that TaLSECs stimulate the secretion of VEGF in HSCs and, in turn, HSCs promote the migration of LSECs (Figure 1F). Thus, the lack of TaHSCs may reduce the availability of VEGF and the promigratory stimuli for LSECs, leading to impaired vascularization of the growing foci. *Angiogenesis proteome profiler* in TaHSCs revealed increased secretion of angiogenic mediators in vitro. The secretion of osteopontin was increased by 40%, which may facilitate metastatic growth and angiogenesis since osteopontin is involved in several liver pathologies,[37] plays several roles in cancer,[38] and targeting osteopontin reduces aHSC and fibrosis in vivo.[39] Moreover, upregulated Cyr61 may facilitate metastasis, promoting immunosuppression in CRC liver metastasis[40] and facilitating angiogenesis and tumor growth.[41,42]

Regarding immunosuppression, TaLSEC-activated HSCs, and TaHSCs increased VEGF, IL-6, and CXCL12 secretion, known to promote the recruitment of MDSC,[17,28,42] which impede the antitumor immune response of lymphocytes, which may be taking place in our model. Therefore, it is tempting to hypothesize that fewer aHSCs may produce lower levels of these soluble signals, leading to decreased MDSC counts, as observed in our model, impairing liver metastasis.[4] Interestingly, CXCL4 and CXCL1 secretion increased in TaHSCs, which mediates the induction of MDSC while favoring their accumulation and proliferation in the premetastatic niche.[43–45]

In conclusion, we uncover a prometastatic role of tumor-reactive HSCs during liver metastasis from different primary origins as an organ-specific response to invading cells. These findings reinforce HSCs as a potential target for new therapies sensitizing the tumor microenvironment to emerging antitumor approaches.

FUNDING INFORMATION

This work was supported by a research grant from Fundación Jesus de Gangoiti Barrera to A.B, GIU20/035 from the University of the Basque Country and IT1275-19 and IT1524-22 from the Basque Government.

CONFLICTS OF INTEREST

The authors have no conflicts to report.

ORCID

Aitor Benedicto https://orcid.org/0000–0002–3026–7190
Alba Herrero https://orcid.org/0000–0002–7436–1605
Aritz Lopategi https://orcid.org/0000–0001–6501–1788
Scott Laurence Friedman https://orcid.org/0000–0003–1178–6195
Maria Dolores Boyano https://orcid.org/0000–0001–6051–1054
Beatriz Arteta https://orcid.org/0000–0003–3253–3162

REFERENCES

1. Tsuchida T, Friedman SL. Mechanisms of hepatic stellate cell activation. Nat Rev Gastroenterol Hepatol. 2017;14:397–411.
2. Puche JE, Lee YA, Jiao J, Aloman C, Fiel MI, Muñoz U, et al. A novel murine model to deplete hepatic stellate cells uncovers their role in amplifying liver damage in mice. Hepatology. 2013;57:339–50.
3. Olaso E, Salado C, Egilegor E, Gutierrez V, Santisteban A, Sancho-Bru P, et al. Proangiogenic role of tumor-activated hepatic stellate cells in experimental melanoma metastasis. Hepatology. 2003;37:674–85.
4. Benedicto A, Romayor I, Arteta B. CXCR4 receptor blockage reduces the contribution of tumor and stromal cells to the metastatic growth in the liver. Oncol Rep. 2018;39:2022–30.
5. Romayor I, Badiola I, Benedicto A, Márquez J, Herrero A, Arteta B, et al. Silencing of sinusoidal DDR1 reduces murine liver metastasis by colon carcinoma. Sci Rep. 2020;10:18398.
6. Cogliati B, Yashaswini CN, Wang S, Sia D, Friedman SL. Friend or foe? The elusive role of hepatic stellate cells in liver cancer. Nat Rev Gastroenterol Hepatol. 2023;20:647–61.
7. Filliol A, Saito Y, Nair A, Dapito DH, Yu LX, Ravichandra A, et al. Opposing roles of hepatic stellate cell subpopulations in hepatocarcinogenesis. Nature. 2022;610:356–65.
8. Zhao S, Mi Y, Zheng B, Wei P, Gu Y, Zhang Z, et al. Highly-metastatic colorectal cancer cell released miR-181a-5p-rich extracellular vesicles promote liver metastasis by activating hepatic stellate cells and remodelling the tumour microenvironment. J Extracell Vesicles. 2022;11:e12186.
9. Dudgeon C, Casabianca A, Harris C, Ogier C, Bellina M, Fiore S, et al. Netrin-1 feedforward mechanism promotes pancreatic cancer liver metastasis via hepatic stellate cell activation, retinoid, and ELF3 signaling. Cell Rep. 2023;42:113369.
10. Ren C, Yang Z, Xu E, Kang X, Wang X, Sun Q, et al. Cross-talk between gastric cancer and hepatic stellate cells promotes invadopodia formation during liver metastasis. Cancer Sci. 2024;115:369–84.
11. Arteta B, Lasuen N, Lopategi A, Sveinbjörnsson B, Smedsrød B, Vidal-Vanaclocha F. Colon carcinoma cell interaction with liver sinusoidal endothelium inhibits organ-specific antitumor immunity through interleukin-1-induced mannose receptor in mice. Hepatology. 2010;51:2172–82.
12. Benedicto A, Herrero A, Romayor I, Marquez J, Smedsrød B, Olaso E, et al. Liver sinusoidal endothelial cell ICAM-1 mediated tumor/endothelial crosstalk drives the development of liver metastasis by initiating inflammatory and angiogenic responses. Sci Rep. 2019;9:13111.
13. Friedman SL. Hepatic stellate cells: Protean, multifunctional, and enigmatic cells of the liver. Physiol Rev. 2008;88:125–72.
14. Jiang X, Wang J, Deng X, Xiong F, Zhang S, Gong Z, et al. The role of microenvironment in tumor angiogenesis. J Exp Clin Cancer Res. 2020;39:204.

15. Fujita T, Narumiya S. Roles of hepatic stellate cells in liver inflammation: A new perspective. Inflamm Regen. 2016;36:1.
16. Blavier L, Nakata R, Neviani P, Sharma K, Shimada H, Benedicto A, et al. The capture of extracellular vesicles endogenously released by xenotransplanted tumours induces an inflammatory reaction in the premetastatic niche. J Extracell Vesicles. 2023;12:e12326.
17. Xu Y, Fang F, Jiao H, Zheng X, Huang L, Yi X, et al. Activated hepatic stellate cells regulate MDSC migration through the SDF-1/CXCR4 axis in an orthotopic mouse model of hepatocellular carcinoma. Cancer Immunol Immunother. 2019;68:1959–69.
18. Douglass A, Wallace K, Parr R, Park J, Durward E, Broadbent I, et al. Antibody-targeted myofibroblast apoptosis reduces fibrosis during sustained liver injury. J Hepatol. 2008;49:88–98.
19. Wallace MC, Friedman SL. Hepatic fibrosis and the microenvironment: fertile soil for hepatocellular carcinoma development. Gene Expr. 2014;16:77–84.
20. Olaso E, Benedicto A, Lopategi A, Cossio FP, Arteta B. A synthetic analog of resveratrol inhibits the proangiogenic response of liver sinusoidal cells during hepatic metastasis. Biomol Ther (Seoul). 2022;30:162–9.
21. Carloni V, Luong TV, Rombouts K. Hepatic stellate cells and extracellular matrix in hepatocellular carcinoma: More complicated than ever. Liver Int. 2014;34:834–43.
22. Wang PW, Lin TY, Yang PM, Yeh CT, Pan TL. Hepatic stellate cell modulates the immune microenvironment in the progression of hepatocellular carcinoma. Int J Mol Sci. 2022;23:10777.
23. Asada S, Kaji K, Nishimura N, Koizumi A, Matsuda T, Tanaka M, et al. Tofogliflozin delays portal hypertension and hepatic fibrosis by inhibiting sinusoidal capillarization in cirrhotic rats. Cells. 2024;13:538.
24. Luo J, Liang Y, Kong F, Qiu J, Liu X, Chen A, et al. Vascular endothelial growth factor promotes the activation of hepatic stellate cells in chronic schistosomiasis. Immunol Cell Biol. 2017;95:399–407.
25. Bush TG, Savidge TC, Freeman TC, Cox HJ, Campbell EA, Mucke L, et al. Fulminant jejuno-ileitis following ablation of enteric glia in adult transgenic mice. Cell. 1998;93:189–201.
26. Spina A, De Pasquale V, Cerulo G, Cocchiaro P, Della Morte R, Avallone L, et al. HGF/c-MET axis in tumor microenvironment and metastasis formation. Biomedicines. 2015;3:71–88.
27. Kang MJ, Lee S, Jung U, Mandal C, Park H, Stetler-Stevenson WG, et al. Inhibition of hepatic stellate cell activation suppresses tumorigenicity of hepatocellular carcinoma in mice. Am J Pathol. 2021;191:2219–30.
28. Chen Y, Qian B, Sun X, Kang Z, Huang Z, Ding Z, et al. Sox9/INHBB axis-mediated crosstalk between the hepatoma and hepatic stellate cells promotes the metastasis of hepatocellular carcinoma. Cancer Lett. 2021;499:243–54.
29. Li F, Zhan L, Dong Q, Wang Q, Wang Y, Li X, et al. Tumor-derived exosome-educated hepatic stellate cells regulate lactate metabolism of hypoxic colorectal tumor cells via the IL-6/STAT3 pathway to confer drug resistance. Onco Targets Ther. 2020;13:7851–64.
30. Deng L, Li T, Liao Y, Liu S, Xie Z, Huang Z, et al. Peritumoral activated hepatic stellate cells are associated with hepatic recurrence for resectable colorectal adenocarcinoma liver metastasis following resection. Oncol Lett. 2020;20:287.
31. Sato Y, Murase K, Kato J, Kobune M, Sato T, Kawano Y, et al. Resolution of liver cirrhosis using vitamin A-coupled liposomes to deliver siRNA against a collagen-specific chaperone. Nat Biotechnol. 2008;26:431–42.
32. Yang MC, Wang CJ, Liao PC, Yen CJ, Shan YS. Hepatic stellate cells secretes type I collagen to trigger epithelial mesenchymal transition of hepatoma cells. Am J Cancer Res. 2014;4:751–63.
33. Geerts A. History, heterogeneity, developmental biology, and functions of quiescent hepatic stellate cells. Semin Liver Dis. 2001;21:311–35.
34. Olaso E, Benedicto A, Lopategi A, Cossio FP, Arteta B. A synthetic analog of resveratrol inhibits the proangiogenic response of liver sinusoidal cells during hepatic metastasis. Biomol Ther (Seoul). 2022;30:162–9.
35. Seandel M, Noack-Kunnmann K, Zhu D, Aimes RT, Quigley JP. Growth factor-induced angiogenesis in vivo requires specific cleavage of fibrillar type I collagen. Blood. 2001;97:2323–32.
36. Takeuchi H, Hashimoto N, Kitai R, Kubota T, Kikuta K. Proliferation of vascular smooth muscle cells in glioblastoma multiforme. J Neurosurg. 2010;113:218–24.
37. Nagoshi S. Osteopontin: Versatile modulator of liver diseases. Hepatol Res. 2014;44:22–30.
38. Yan Z, Hu X, Tang B, Deng F. Role of osteopontin in cancer development and treatment. Heliyon. 2023;9:e21055.
39. Tang M, Guo C, Sun M, Zhou H, Peng X, Dai J, et al. Effective delivery of osteopontin small interference RNA using exosomes suppresses liver fibrosis via TGF-β1 signaling. Front Pharmacol. 2022;13:882243.
40. Wang Z, Kim SY, Tu W, Kim J, Xu A, Yang YM, et al. Extracellular vesicles in fatty liver promote a metastatic tumor microenvironment. Cell Metab. 2023;35:1209–226.e13.
41. Babic AM, Kireeva ML, Kolesnikova TV, Lau LF. CYR61, a product of a growth factor-inducible immediate early gene, promotes angiogenesis and tumor growth. Proc Natl Acad Sci U S A. 1998;95:6355–60.
42. Tsai MS, Bogart DF, Castañeda JM, Li P, Lupu R. Cyr61 promotes breast tumorigenesis and cancer progression. Oncogene. 2002;21:8178–85.
43. Horikawa N, Abiko K, Matsumura N, Hamanishi J, Baba T, Yamaguchi K, et al. Expression of vascular endothelial growth factor in ovarian cancer inhibits tumor immunity through the accumulation of myeloid-derived suppressor cells. Clin Cancer Res. 2017;23:587–99.
44. Joseph R, Soundararajan R, Vasaikar S, Yang F, Allton KL, Tian L, et al. CD8+ T cells inhibit metastasis and CXCL4 regulates its function. Br J Cancer. 2021;125:176–89.
45. Zheng Y, Wang N, Wang S, Zhang J, Yang B, Wang Z. Chronic psychological stress promotes breast cancer pre-metastatic niche formation by mobilizing splenic MDSCs via TAM/CXCL1 signaling. J Exp Clin Cancer Res. 2023;42:129.

How to cite this article: Benedicto A, Herrero A, Lopategi A, Friedman SL, Boyano MD, Arteta B. Depletion of tumor-reactive HSCs reveals their significance during different stages of liver metastasis. Hepatol Commun. 2025;9:e0669. https://doi.org/10.1097/HC9.0000000000000669